Zeitschrift: Helvetica Physica Acta
Band: 44 (1971)
Heft: 2

Artikel: Calculation of the multiplicity yield function of the IGY neutron monitor
Autor: Debrunner, H. / Flückiger, E.
DOI: https://doi.org/10.5169/seals-114280

Calculation of the Multiplicity Yield Function of the IGY Neutron Monitor[1])

by **H. Debrunner** and **E. Flückiger**

Physikalisches Institut, University of Berne,
Berne, Switzerland

(11. IX. 70)

Abstract. Calculations to determine the multiplicity response function for IGY neutron monitors are reported for vertically incident primary cosmic ray protons of the rigidity range 2.2 GV $< R_0 <$ 100 GV. A Monte Carlo method is used to calculate the secondary nucleon flux intensities in the atmosphere. Empirical and theoretical data on neutron monitor response are employed to relate the calculated flux data to the counting rates of the various multiplicities.

A direct comparison of our multiplicity response function and other related quantities with experimental data is at present not yet possible. But indirect comparisons show fairly good agreement.

1. Introduction

The multiplicity spectrum of neutron monitors reflects the energy spectrum of the primary cosmic radiation striking the atmosphere above the monitor. In principle, multiplicity measurements therefore offer the possibility of observing primary cosmic ray variations even during magnetic storms, and at rigidities above the equatorial threshold rigidity. But for these analyses one must know the correlation between the primary cosmic radiation at the top of the atmosphere and the observed multiplicity spectrum in the monitor. In an attempt to determine this correlation, the multiplicity yield function of neutron monitors is being calculated.

The method of calculation was described in detail in previous papers [1–4]. A Monte Carlo program simulates the development of the nucleonic cascade in the atmosphere and determines $\overline{N}_{kij}(h, R_0, \vartheta_0)$, i.e. the average number of nucleons of type k (neutrons and protons), in the kinetic energy interval ΔE_i, the zenith angle element $\Delta\vartheta_j$, and at the atmospheric depth h, which is produced by a primary proton of rigidity R_0 and zenith angle ϑ_0 penetrating the atmosphere. This part of the calculation has been tested by integrating the differential spectra of secondary protons over the rigidity spectrum and solid angle of the primary radiation, and comparing the results with measured proton spectra at $h = 850$ g cm^{-2} and 1033 g cm^{-2}. The agreement between the theoretical and the experimental data is good [1, 2].

---

[1]) Presented at the Second European Symposium on Cosmic Rays-Modulation Effects, Amsterdam, August 31st–September 4th, 1970.

The probability that a primary proton will produce a secondary nucleon with the parameters (k, i, j) striking a neutron monitor in the atmospheric depth h then is

$$P_{kij}(h, R_0, \vartheta_0) = \frac{\bar{N}_{kij}(h, R_0, \vartheta_0)}{\sum_k \sum_i \sum_j \bar{N}_{kij}(h, R_0, \vartheta_0)} \cdot \left[1 - \exp\left(- \sum_k \sum_i \sum_j \bar{N}_{kij}(h, R_0, \vartheta_0)\right)\right]. \quad (1)$$

Here it is assumed that the secondary nucleons of a cascade reaching the surface of the earth are not correlated with each other – a reasonable assumption for moderate primary rigidities – and that their number follows a Poisson distribution. Allowance is also made for the fact that the area of neutron monitors is small compared with the spread of nucleonic cascades.

For a description of the response of the monitor to the secondary radiation incident upon it, we follow Cocconi et al. [5], Hughes et al. [6], Shen [7] and Nobles et al. [8]. The probability that a neutron or a proton of the energy E_i, penetrating normally a layer of lead of thickness T (measured in units of the mean free path) and interacting with the lead, will produce ν low energy neutrons is taken to be

$$I_k(\nu, E_i, T) = \frac{1}{\bar{\nu}_k(E_i, T) + 1} \left(\frac{\bar{\nu}_k(E_i, T)}{\bar{\nu}_k(E_i, T) + 1}\right)^{\nu}. \quad (2)$$

For the average number of neutrons produced, $\bar{\nu}_k(E_i, T)$, we have used the values of Shen [7].

The probability of detecting the multiplicity m in an event with ν low energy neutrons is given by

$$W_m^{\nu} = \binom{\nu}{m} \varepsilon^m f^{m-1} \sum_{s=0}^{\nu-m} \frac{m}{s+m} \cdot \binom{\nu - m}{s} \cdot (1 - \varepsilon)^{\nu-m-s} [\varepsilon (1 - f)]^s \quad (3)$$

where ε is the neutron detection probability and f the gate efficiency taking into account the limited active time of multiplicity meters.

Finally the irregular structure of the lead core has to be considered. This is done by introducing the azimuth angles, φ_l, and by attributing to each direction (j, l) the gradually varying and weighted thickness of lead, T_{jln}.

The multiplicity yield function is then given by

$$F(m, h, R_0, \vartheta_0) = \sum_k \sum_i \sum_j \sum_l \sum_n \alpha_{jln} [1 - \exp(-T_{jln})] \cdot P_{kij}(h, R_0, \vartheta_0) \sum_{\nu=m}^{\infty} I_k(\nu, E_i, T_{jln}) W_m^{\nu}. \quad (4)$$

2. First Results

In order to check our method of analysis we have started to determine the multiplicity yield function of the IGY neutron monitor. In these first calculations, we have neglected the contribution of muons to the counting rate and the influence

of the paraffin on the production of evaporation neutrons. However, in a more sophisticated version of the program, these effects will be taken into account.

Thus far, the multiplicity yield function has been calculated for the following parameters:

$1 \leqslant m \leqslant 20$,
$h = 650$ g cm^{-2} (altitude of the Jungfraujoch station) and 1033 g cm^{-2} (sea level),
$R_0 = 2.2$, 3.15, 4.37, 5.74, 7.73, 10.5, 20, 50 and 100 GV,
$\vartheta_0 = 0°$.

In the numerical integrations over i, j, l and n, the energy range of the secondaries, 50 MeV $\leqslant E \leqslant$ 100 GeV, has been divided into 21 intervals and the solid angle into 40 elements. For the various directions of incidence, (j, l), up to 7 different thicknesses of lead have been used. Following Harman and Hatton [9] we have adopted a neutron detection probability of $\varepsilon = 0.02$. The gate efficiency, f, was estimated as 0.918.

The results of these analysis are shown in Tables 1 and 2.

In order to simplify the discussion, the more commonly used multiplicity response function has been derived by multiplying the yield function with the area of the monitor, $S \cdot \cos\vartheta_0$, and the differential rigidity spectrum of the primary radiation, $\psi(R_0)$:

$$K_{IGY}(m, h, R_0, \vartheta_0) = S \cdot \cos\vartheta_0 \cdot \psi(R_0) \cdot F_{IGY}(m, h, R_0, \vartheta_0) \ . \tag{5}$$

For the area, one section of the IGY-neutron monitor with six counters has been used. For the average spectrum of primary protons we have taken the values listed in Table 3. The results are presented in Figures 1 and 2. They show that the slopes of the various multiplicity response functions differ from each other for rigidities $R_0 \leqslant 20$ GV and that the rigidity of the maximum response increases with increasing multiplicity and increasing atmospheric depth. The numerical values show that the multiplicity spectrum of IGY neutron monitors can be used – at least theoretically – to analyse primary cosmic ray variations up to $R_0 \leqslant 20$ GV.

The response function of the total counting rate has also been calculated. It is given by

$$K_{IGY}(h, R_0, \vartheta_0) = \sum_{m=1}^{\infty} m \cdot K_{IGY}(m, h, R_0, \vartheta_0) \tag{6}$$

and is shown in Figure 3. Its slope is similar to that of the multiplicity response function of $m = 1$.

Other quantities of interest are the ratios of the various multiplicities, the mean multiplicity, and the barometric coefficients. The ratios of multiplicities are obtained by integrating the various multiplicity response functions over the primary rigidities. They are listed as a function of threshold rigidity in the Tables 4 and 5. The mean multiplicity is obtained by averaging the multiplicities weighted by their counting rates. It is shown in Figure 4. The barometric coefficients of multiplicities $m = 1$, 2, 4 and 8 are deduced from the counting rates of the different multiplicities at $h =$ 650 g cm^{-2} and 1033 g cm^{-2} and therefore refer to an average atmospheric depth of $h \approx 850$ g cm^{-2}. Their dependence on threshold rigidity is plotted in Figure 5.

Table 1

Multiplicity yield function of the IGY neutron monitor, $F(m, h = 650\ \mathrm{g\ cm^{-2}}, R_0, \vartheta_0 = 0°)$, in counts per primary proton

R_0 / m	2.2 GV	3.15 GV	4.37 GV	5.74 GV	7.73 GV	10.5 GV	20 GV	50 GV	100 GV
1	$1.12 \cdot 10^{-3}$	$4.20 \cdot 10^{-3}$	$1.17 \cdot 10^{-2}$	$1.65 \cdot 10^{-2}$	$2.40 \cdot 10^{-2}$	$3.05 \cdot 10^{-2}$	$4.13 \cdot 10^{-2}$	$5.62 \cdot 10^{-2}$	$6.37 \cdot 10^{-2}$
2	$1.98 \cdot 10^{-4}$	$8.19 \cdot 10^{-4}$	$2.67 \cdot 10^{-3}$	$4.05 \cdot 10^{-3}$	$6.24 \cdot 10^{-3}$	$8.71 \cdot 10^{-3}$	$1.22 \cdot 10^{-2}$	$1.61 \cdot 10^{-2}$	$1.87 \cdot 10^{-2}$
3	$3.69 \cdot 10^{-5}$	$1.77 \cdot 10^{-4}$	$7.17 \cdot 10^{-4}$	$1.23 \cdot 10^{-3}$	$2.03 \cdot 10^{-3}$	$3.12 \cdot 10^{-3}$	$4.55 \cdot 10^{-3}$	$5.90 \cdot 10^{-3}$	$7.10 \cdot 10^{-3}$
4	$7.28 \cdot 10^{-6}$	$4.27 \cdot 10^{-5}$	$2.25 \cdot 10^{-4}$	$4.51 \cdot 10^{-4}$	$8.00 \cdot 10^{-4}$	$1.32 \cdot 10^{-3}$	$2.04 \cdot 10^{-3}$	$2.64 \cdot 10^{-3}$	$3.27 \cdot 10^{-3}$
5	$1.52 \cdot 10^{-6}$	$1.16 \cdot 10^{-5}$	$8.04 \cdot 10^{-5}$	$1.90 \cdot 10^{-4}$	$3.58 \cdot 10^{-4}$	$6.22 \cdot 10^{-4}$	$1.02 \cdot 10^{-3}$	$1.33 \cdot 10^{-3}$	$1.70 \cdot 10^{-}$
6	$3.32 \cdot 10^{-7}$	$3.52 \cdot 10^{-6}$	$3.16 \cdot 10^{-5}$	$8.73 \cdot 10^{-5}$	$1.74 \cdot 10^{-4}$	$3.13 \cdot 10^{-4}$	$5.47 \cdot 10^{-4}$	$7.26 \cdot 10^{-4}$	$9.51 \cdot 10^{-4}$
7	$7.61 \cdot 10^{-8}$	$1.19 \cdot 10^{-6}$	$1.33 \cdot 10^{-5}$	$4.24 \cdot 10^{-5}$	$8.92 \cdot 10^{-5}$	$1.65 \cdot 10^{-4}$	$3.07 \cdot 10^{-4}$	$4.15 \cdot 10^{-4}$	$5.58 \cdot 10^{-4}$
8	$1.82 \cdot 10^{-8}$	$4.36 \cdot 10^{-7}$	$5.88 \cdot 10^{-6}$	$2.14 \cdot 10^{-5}$	$4.73 \cdot 10^{-5}$	$8.91 \cdot 10^{-5}$	$1.78 \cdot 10^{-4}$	$2.47 \cdot 10^{-4}$	$3.40 \cdot 10^{-4}$
9	$4.54 \cdot 10^{-9}$	$1.72 \cdot 10^{-7}$	$2.69 \cdot 10^{-6}$	$1.11 \cdot 10^{-5}$	$2.57 \cdot 10^{-5}$	$4.93 \cdot 10^{-5}$	$1.06 \cdot 10^{-4}$	$1.51 \cdot 10^{-4}$	$2.14 \cdot 10^{-4}$
10	$1.17 \cdot 10^{-9}$	$7.18 \cdot 10^{-8}$	$1.26 \cdot 10^{-6}$	$5.84 \cdot 10^{-6}$	$1.43 \cdot 10^{-5}$	$2.79 \cdot 10^{-5}$	$6.48 \cdot 10^{-5}$	$9.45 \cdot 10^{-5}$	$1.39 \cdot 10^{-4}$

Table 2

Multiplicity yield function of the IGY neutron monitor, $F(m, h = 1033\ \mathrm{g\ cm^{-2}}, R_0, \vartheta_0 = 0°)$, in counts per primary proton

R_0 / m	2.2 GV	3.15 GV	4.37 GV	5.74 GV	7.73 GV	10.5 GV	20 GV	50 GV	100 GV
1	$1.94 \cdot 10^{-5}$	$1.97 \cdot 10^{-4}$	$4.83 \cdot 10^{-4}$	$1.42 \cdot 10^{-3}$	$2.80 \cdot 10^{-3}$	$3.64 \cdot 10^{-3}$	$7.17 \cdot 10^{-3}$	$1.13 \cdot 10^{-2}$	$1.63 \cdot 10^{-2}$
2	$3.38 \cdot 10^{-6}$	$3.30 \cdot 10^{-5}$	$9.67 \cdot 10^{-5}$	$3.40 \cdot 10^{-4}$	$6.35 \cdot 10^{-4}$	$8.75 \cdot 10^{-4}$	$1.92 \cdot 10^{-3}$	$2.96 \cdot 10^{-3}$	$4.32 \cdot 10^{-3}$
3	$5.93 \cdot 10^{-7}$	$5.83 \cdot 10^{-6}$	$2.28 \cdot 10^{-5}$	$9.75 \cdot 10^{-5}$	$1.75 \cdot 10^{-4}$	$2.57 \cdot 10^{-4}$	$6.46 \cdot 10^{-4}$	$9.76 \cdot 10^{-4}$	$1.44 \cdot 10^{-3}$
4	$1.06 \cdot 10^{-7}$	$1.10 \cdot 10^{-6}$	$6.50 \cdot 10^{-6}$	$3.31 \cdot 10^{-5}$	$5.78 \cdot 10^{-5}$	$9.09 \cdot 10^{-5}$	$2.64 \cdot 10^{-4}$	$3.93 \cdot 10^{-4}$	$5.77 \cdot 10^{-4}$
5	$1.91 \cdot 10^{-8}$	$2.19 \cdot 10^{-7}$	$2.23 \cdot 10^{-6}$	$1.28 \cdot 10^{-5}$	$2.21 \cdot 10^{-5}$	$3.70 \cdot 10^{-5}$	$1.24 \cdot 10^{-4}$	$1.81 \cdot 10^{-4}$	$2.59 \cdot 10^{-4}$
6	$3.50 \cdot 10^{-9}$	$4.64 \cdot 10^{-8}$	$8.85 \cdot 10^{-7}$	$5.35 \cdot 10^{-6}$	$9.36 \cdot 10^{-6}$	$1.65 \cdot 10^{-5}$	$6.30 \cdot 10^{-5}$	$9.05 \cdot 10^{-5}$	$1.25 \cdot 10^{-4}$
7	$6.51 \cdot 10^{-10}$	$1.04 \cdot 10^{-8}$	$3.85 \cdot 10^{-7}$	$2.37 \cdot 10^{-6}$	$4.22 \cdot 10^{-6}$	$7.74 \cdot 10^{-6}$	$3.39 \cdot 10^{-5}$	$4.77 \cdot 10^{-5}$	$6.31 \cdot 10^{-5}$
8	$1.23 \cdot 10^{-10}$	$2.43 \cdot 10^{-9}$	$1.76 \cdot 10^{-7}$	$1.08 \cdot 10^{-6}$	$1.99 \cdot 10^{-6}$	$3.77 \cdot 10^{-6}$	$1.90 \cdot 10^{-5}$	$2.61 \cdot 10^{-5}$	$3.30 \cdot 10^{-5}$
9	$2.34 \cdot 10^{-11}$	$5.93 \cdot 10^{-10}$	$8.34 \cdot 10^{-8}$	$5.08 \cdot 10^{-7}$	$9.64 \cdot 10^{-7}$	$1.88 \cdot 10^{-6}$	$1.10 \cdot 10^{-5}$	$1.46 \cdot 10^{-5}$	$1.77 \cdot 10^{-5}$
10	$4.54 \cdot 10^{-12}$	$1.49 \cdot 10^{-10}$	$4.02 \cdot 10^{-8}$	$2.42 \cdot 10^{-7}$	$4.79 \cdot 10^{-7}$	$9.52 \cdot 10^{-7}$	$6.48 \cdot 10^{-6}$	$8.38 \cdot 10^{-6}$	$9.70 \cdot 10^{-6}$

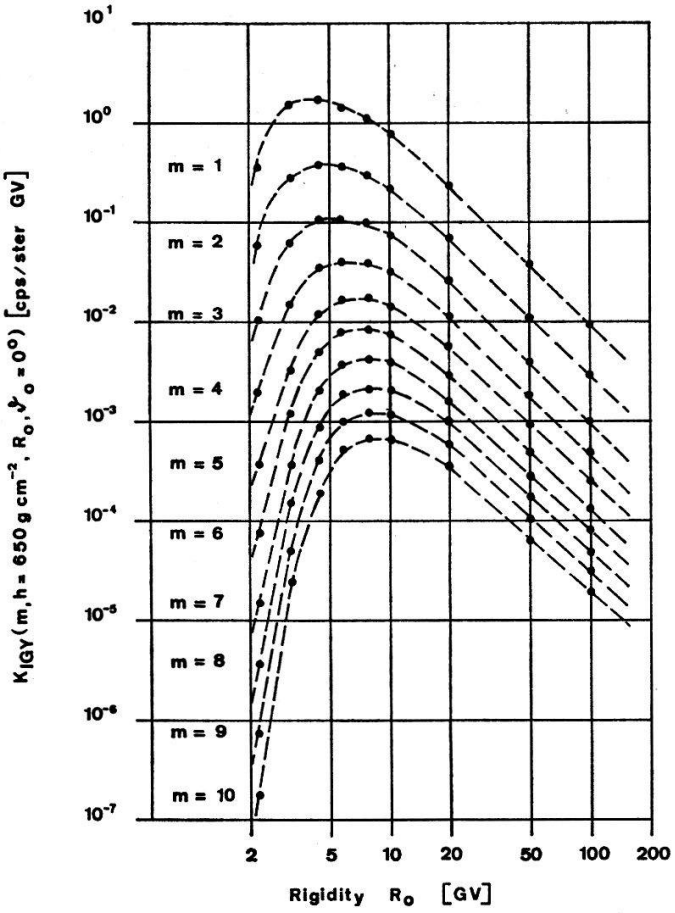

Figure 1
Multiplicity response function of the IGY neutron monitor for h = 650 g cm^{-2} and $\vartheta_0 = 0°$.

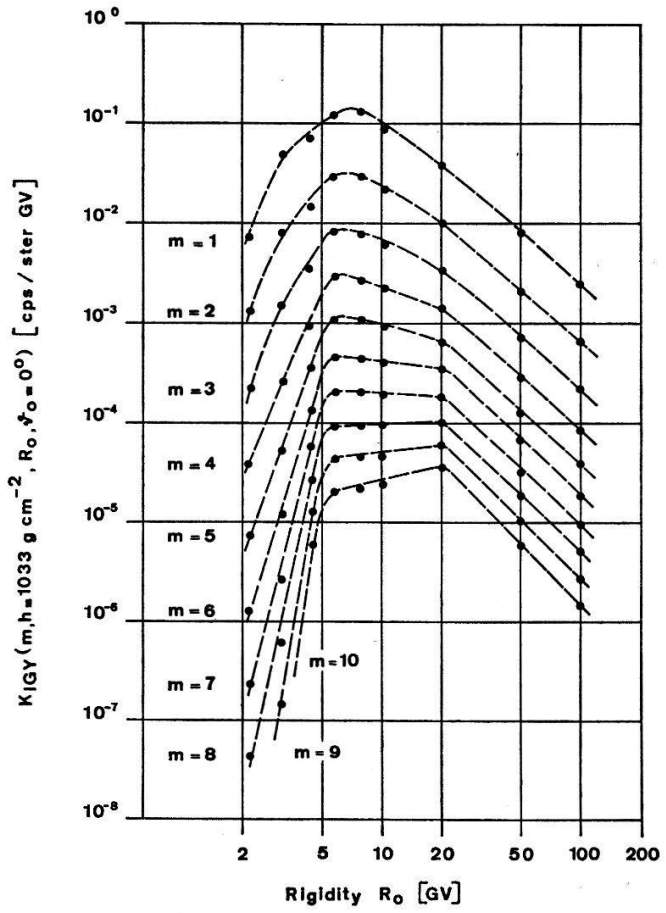

Figure 2
Multiplicity response function of the IGY neutron monitor for h = 1033 g cm^{-2} and $\vartheta_0 = 0°$.

3. Discussion

It should be noted at the outset that our present results refer only to vertically incident primary radiation. On the other hand, all experimental data concerning the yield function, the response function, the ratios of various multiplicities and the barometric coefficients of IGY neutron monitors are related to omnidirectional primary radiation. Therefore, a direct comparison of our results with measurements is not yet possible.

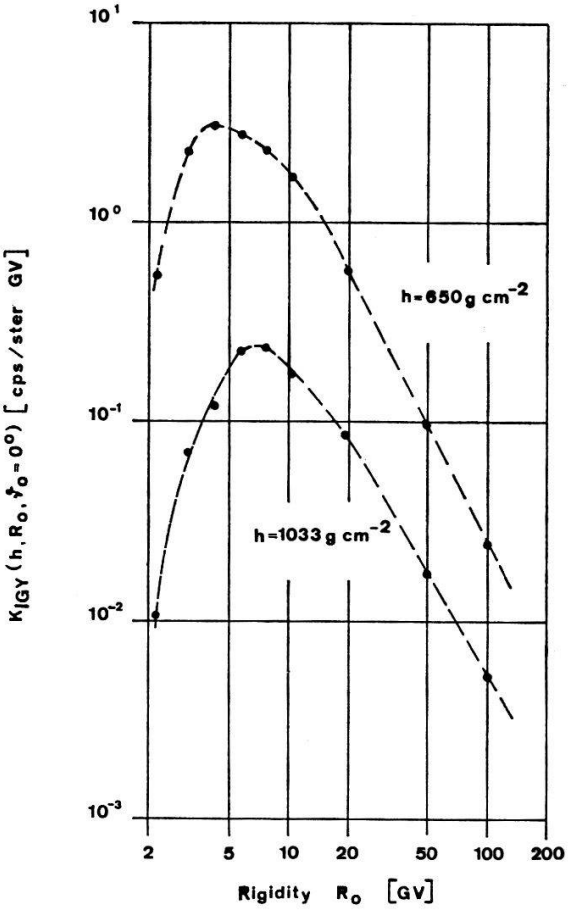

Figure 3
Response function of the total counting rate of the IGY neutron monitor for h = 650 and 1033 g cm^{-2} and $\vartheta_0 = 0°$.

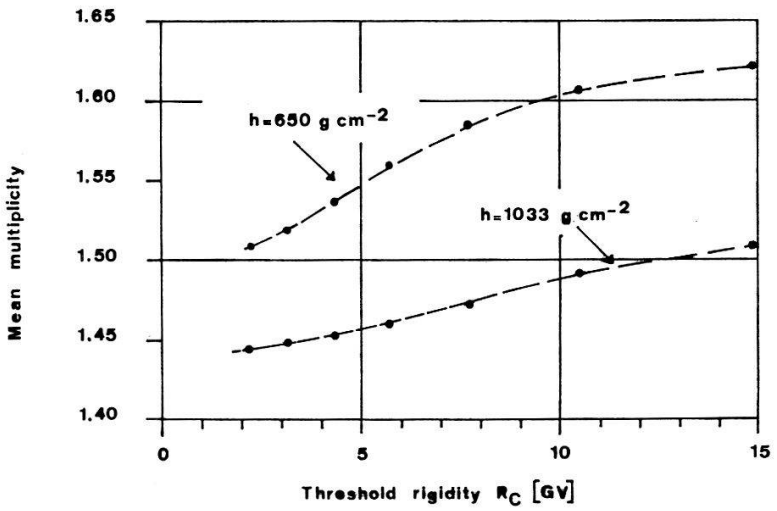

Figure 4
Mean multiplicity of the IGY neutron monitor for vertically incident primary radiation as a function of threshold rigidity.

However, indirect comparisons can be made. In Figure 6 the calculated vertical total response function, $K(h, R_0, \vartheta_0)$, of an IGY neutron monitor at $h = 650$ g cm^{-2} is shown with the omnidirectional total response function, $V(h, R_0, R_C)$, experimentally determined by Dorman [10] for an IGY neutron monitor at $h = 700$ g cm^{-2} and with the threshold rigidity $R_C = 4.48$ GV. The slopes of the two curves are similar. Apparently our analysis is the first theoretical approach to the response function of neutron monitors that describes conditions over two orders of magnitude of the primary rigidity at least qualitatively.

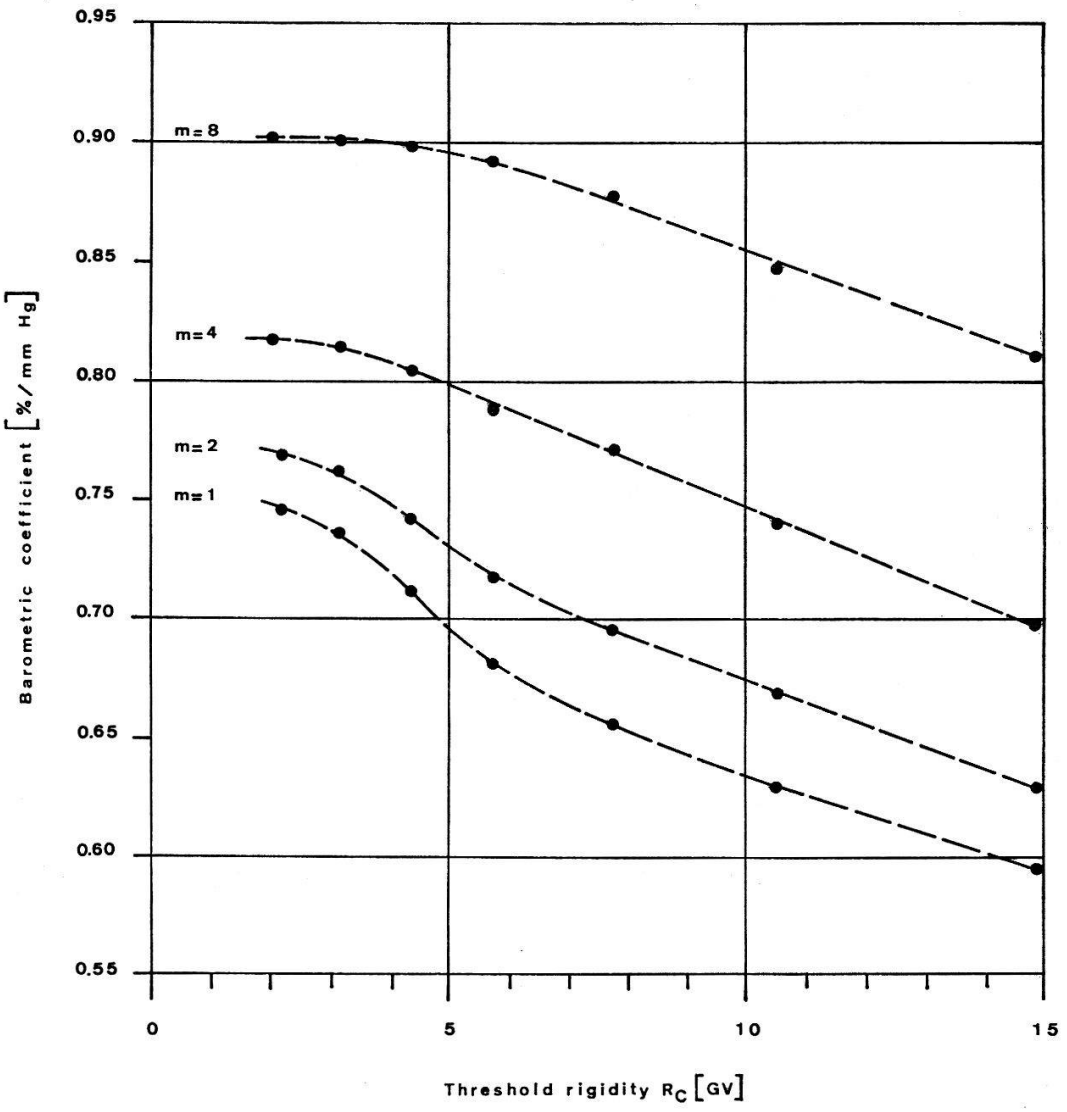

Figure 5
Barometric coefficients of multiplicities $m = 1, 2, 4$ and 8 as a function of threshold rigidity. The data refer to the atmospheric depth of $h = 850$ g cm^{-2} and to vertically incident primary radiation.

For a quantitative comparison, we relate our response function to that of Dorman by assuming a potential law in $\cos\vartheta_0$ for the dependence of the unidirectional response function on primary zenith angle:

$$V(h, R_0, R_C) = \frac{2\pi}{Z(h, R_C)} \int_0^{\pi/2} K(h, R_0 > R_C, \vartheta_0 = 0^\circ) \cdot \cos^n\vartheta_0 \cdot \cos\vartheta_0 \cdot \sin\vartheta_0 \cdot d\vartheta_0 , \qquad (7)$$

where $Z(h, R_C)$ is the total counting rate of a monitor with parameters h and R_C. In the numerical evaluation we adopted for $Z(h, R_C)$ the total counting rate of our IGY neutron monitor at Jungfraujoch. The exponent, n, then turns out to be of the order of 3.5 at lower primary rigidities and to decrease with increasing rigidity as shown in Table 6. Our values for $R_0 \leqslant 20$ GV lie between the theoretical result of Rao et al. [11] and the experimental one of Phillips and Parsons [12]. The decrease of n with increasing rigidity is expected, because cascades produced by primaries of higher rigidity have to pass through more matter to reach equilibrium between low energy and high energy nucleons. It therefore seems that our analysis can provide even a quantitative description of atmospheric cascade processes and the response of neutron monitors.

Table 3

Assumed differential spectrum of primary protons, $\psi(R_0)$

R_0 [GV]	$\psi(R_0)$ [p/cm^2 ster s GV]
2.2	$3.9 \cdot 10^{-2}$
3.15	$2.6 \cdot 10^{-2}$
4.37	$1.6 \cdot 10^{-2}$
5.74	$9.2 \cdot 10^{-3}$
7.73	$5.0 \cdot 10^{-3}$
10.5	$2.6 \cdot 10^{-3}$
20.	$6.0 \cdot 10^{-4}$
50.	$7.5 \cdot 10^{-5}$
100.	$1.6 \cdot 10^{-5}$

Table 4

Ratios of the various multiplicities produced by vertically incident primary radiation as a function of threshold rigidity, Rc, for $h = 650$ g cm^{-2}

R_C →	2.2 GV	3.15 GV	4.37 GV	5.74 GV	7.73 GV	10.5 GV	14.9 GV
Z_2/Z_1	0.265	0.268	0.274	0.280	0.286	0.291	0.292
Z_3/Z_2	0.333	0.337	0.344	0.352	0.360	0.367	0.370
Z_4/Z_3	0.407	0.410	0.418	0.426	0.435	0.443	0.449
Z_5/Z_4	0.467	0.469	0.475	0.482	0.490	0.498	0.505
Z_6/Z_5	0.509	0.510	0.514	0.520	0.526	0.533	0.542
Z_7/Z_6	0.539	0.539	0.543	0.548	0.554	0.561	0.569
Z_8/Z_7	0.565	0.565	0.567	0.572	0.578	0.586	0.597
Z_9/Z_8	0.573	0.573	0.574	0.578	0.582	0.588	0.596
Z_{10}/Z_9	0.585	0.585	0.586	0.589	0.593	0.598	0.606

A very sensitive check would be the comparison between measured and calculated ratios of various multiplicities. For lack of directly equivalent data, Table 7 compares our unidirectional results with observed data at Jungfraujoch [13] and Leeds [14]. The Leeds data refer only to neutrons detected as a result of nucleon interactions in the lead of the monitor, since the contribution of neutrons produced in the paraffin or from pions and muons has been removed. The comparison of the calculated and experimental values shows that our ratios are higher than the measured ones for multiplicities $m < 6$ and lower for $m > 7$. In the case of Jungfraujoch, the differences

are presumably due to the paraffin wax surrounding the core of the monitor and the counters and to the contribution of the obliquely incident primary cosmic radiation to the measured counting rates. The paraffin which has not been taken into account by our program affects the multiplicity of nucleons hitting the monitor, reducing it for low energy nucleons and increasing it for high energy nucleons. This means that the ratios Z_{m+1}/Z_m are overestimated by the present program for small multiplicities and underestimated for high multiplicities. A similar effect is found in a comparison of vertically and obliquely incident cascades. At a given atmospheric depth, the mean energy of cascade particles decreases with increasing zenith angle of the cascade. On the other hand, the thickness of lead which a particle can traverse increases with increasing angle of incidence. Thus, the integration of our unidirectional data over the primary zenith angle will lower the ratios for small multiplicities and increase those of high multiplicities. With these arguments in mind the calculated and measured data are not inconsistent with each other. In the case of Leeds the differences can be attributed only to the latter effect. Further calculations for zenith angles different from zero therefore provide a quantitative measure of the reliability of our program.

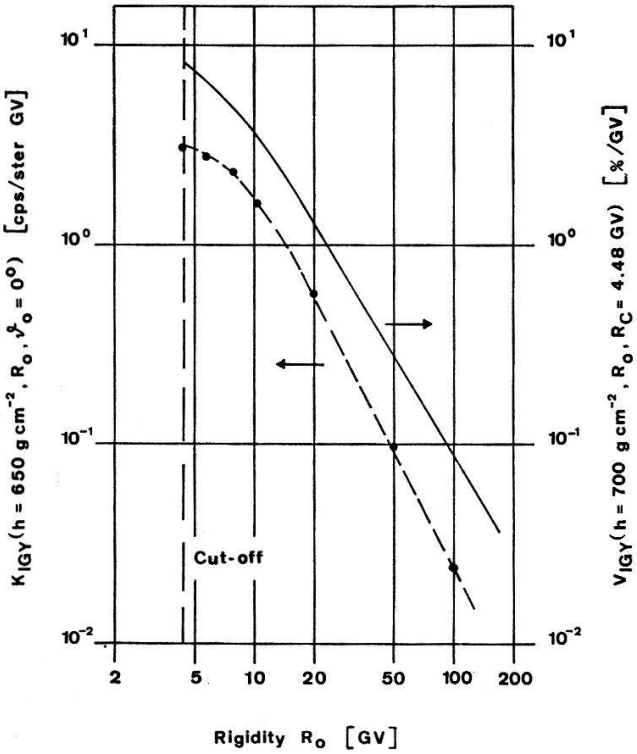

Figure 6
Comparison of the response functions K (h = 650 g cm^{-2} R_0, ϑ_0) and V (h = 700 g cm^{-2}, R_0, R_C = 4.48 GV).

The mean multiplicity, plotted in Figure 4 as a function of threshold rigidity, is very strongly correlated with the multiplicity ratios. Here, too, a direct comparison with experimental data is not yet possible. But indirect comparisons, for instance with the measurements of Dyring and Sporre [15], show qualitative agreement.

The barometric coefficients of multiplicities m = 1, 2, 4 and 8, referring to the atmospheric depth of h = 850 g cm^{-2} and plotted in Figure 5 as a function of threshold rigidity, also agree with the experimental data. The atmospheric attenuation of the cosmic ray intensity increases with increasing multiplicity and decreases with increasing threshold rigidity. From separate calculations, the barometric coefficient of single cascades has been determined. For the multiplicity m = 1 it decreases from 1.44%/mm Hg to 0.48%/mm Hg if the rigidity of the primary proton producing the

cascade increases from 2.2 GV to 100 GV. The corresponding values for $m = 8$ are 1.77%/mm Hg and 0.83%/mm Hg. Integration of our results over the primary solid angle should therefore provide omnidirectional barometric coefficients which agree quantitatively with experimental ones [16].

Table 5

Ratios of the various multiplicities produced by vertically incident primary radiation as a function of threshold rigidity, R_C, for $h = 1033$ g cm^{-2}

R_C	2.2 GV	3.15 GV	4.37 GV	5.74 GV	7.73 GV	10.5 GV	14.9 GV
Z_2/Z_1	0.248	0.249	0.251	0.253	0.256	0.261	0.266
Z_3/Z_2	0.310	0.311	0.314	0.316	0.321	0.328	0.335
Z_4/Z_3	0.382	0.383	0.385	0.388	0.395	0.404	0.411
Z_5/Z_4	0.435	0.436	0.437	0.440	0.445	0.453	0.459
Z_6/Z_5	0.480	0.480	0.481	0.483	0.488	0.495	0.502
Z_7/Z_6	0.508	0.508	0.509	0.511	0.516	0.522	0.526
Z_8/Z_7	0.537	0.537	0.537	0.540	0.545	0.551	0.554
Z_9/Z_8	0.550	0.550	0.550	0.551	0.556	0.561	0.567
Z_{10}/Z_9	0.555	0.555	0.555	0.557	0.560	0.564	0.570

Table 6

The rigidity dependence of the exponent n in equation (7)

R_0 [GV]	n
4.37	3.0
10.5	3.5
20.	3.5
50.	2.5
100.	1.8

Table 7

Comparison between calculated and observed multiplicity ratios at Jungfraujoch and Leeds

Multiplicity ratio	Jungfraujoch		Multiplicity ratio	Leeds	
	calculated	observed		calculated	observed
Z_2/Z_1	0.274	0.159	Z_2/Z_1	0.248	0.206
Z_3/Z_2	0.344	0.247	Z_3/Z_2	0.310	0.224
Z_4/Z_3	0.418	0.330	Z_4/Z_3	0.382	0.301
Z_5/Z_4	0.475	0.367	Z_5/Z_4	0.435	0.397
$(Z_6+Z_7)/Z_5$	0.793	0.804*)	Z_6/Z_5	0.480	0.471
			Z_7/Z_6	0.508	0.541
			Z_8/Z_7	0.537	0.587
			Z_9/Z_8	0.550	0.636

*) Not corrected for overlapping effects.

These indirect comparisons suggest that our program provides a good description of the development of nucleonic cascades in the atmosphere and of the response of neutron monitors. Further calculations should therefore produce yield and response functions for the various types of neutron monitors and increase our knowledge of cosmic ray monitoring.

Acknowledgments

We would like to thank Professor E. Å. Brunberg and Professor J. Geiss for helpful discussions and Professor E. Anders for correcting the English manuscript. We are also grateful to Mrs. U. Brun-Megert for preparing the tables, plotting the figures and typing the paper.

This work was supported in part by the IBM Extension Suisse, by the Deutsches Rechenzentrum Darmstadt, and by the Swiss National Science Foundation.

REFERENCES

[1] H. Debrunner and E. Å. Brunberg, Can J. Phys. *46*, 1069 (1968).
[2] H. Debrunner, Habilitationsarbeit, University of Berne (1968).
[3] H. Debrunner and E. Flückiger, to be published in the Proc. of the 11th International Conference on Cosmic Rays, Budapest (1969).
[4] H. Debrunner and E. Flückiger, Helv. phys. Acta, 43, 509 (1970).
[5] G. Cocconi, V. Cocconi Tongiorgi and M. Widgoff, Phys. Rev. *79*, 768 (1950).
[6] E. B. Hughes, P. L. Marsden, G. Brooke, M. A. Meyer and A. W. Wolfendale, Proc. Phys. Soc. *83*, 239 (1964).
[7] M. L. Shen, Bull. Am. Phys. Soc. *13*, 693 (1968).
[8] R. A. Nobles, R. A. Alber, L. L. Newkirk, M. Walt and C. J. Wolfson, Nucl. Instr. Methods *70*, 45 (1969).
[9] C. V. Harman and C. J. Hatton, Canad. J. Phys. *46*, 1052 (1968).
[10] L. I. Dorman, *Cosmic Ray Variations*, State Publishing House of Technical and Theoretical Literature, Moscow (1957).
[11] U. R. Rao, K. G. McCracken and D. Venkatesan, J. Geophys. Res. *68*, 345 (1963).
[12] J. Phillips and N. R. Parsons, J. Phys. Soc. Japan *17*, 519 (1962).
[13] U. Walther, Lizentiatsarbeit, University of Berne (1967).
[14] E. B. Hughes and P. L. Marsden, J. Geophys. Res. *71*, 1435 (1966).
[15] E. Dyring and B. Sporre, Arkiv Geofysik *5*, 67 (1966).
[16] C. J. Hatton and W. K. Griffiths, J. Geophys. Res. *73*, 7503 (1968).